Supporting information

Electronic Structure Influences on the Formation of the Solid Electrolyte Interphase

Weixin Song,[*1] Elena Stein Scholtis,[1] Peter C. Sherrell,[1,2] D. K. H. Tsang,[1] Jonathan Ngiam,[1] Johannes Lischner,[1] Sarah Fearn,[1] Victoria Bemmer,[1] Cecilia Mattevi,[1] Norbert Klein,[1] Fang Xie,[1] D. Jason Riley*[1]*

[1]*Department of Materials and London Center for Nanotechnology, Imperial College London, UK*

[2]*Department of Chemical Engineering, The University of Melbourne, Parkville, Victoria, Australia*

* jason.riley@imperial.ac.uk

Experimental

Graphene preparation: Copper foils (0.125mm thickness, Sigma-Aldrich) were prepared for graphene synthesis via immersion cleaning in a glacial acetic acid bath for 60 mins prior to growth. The foils were removed from the glacial acetic acid bath and carefully dried with a compressed air jet ensuring no residue remained on the surface. Graphene samples was synthesised using a bespoke VGScientia CVD furnace at a growth temperature set-point of 1050 ^{o}C using methane as the carbon source for 30mins. The copper foils were rotated during growth at 5 rpm to ensure homogenous interactions with the gas flow. Samples were cooled to room temperature naturally under a flow of 200 sccm of argon before removal from the furnace. Mono-layer graphene was synthesized with a H_2:CH_4 ratio of 8:2 at a pressure of 4 torr. Bi-layer graphene was synthesized with a H_2:CH_4 ratio of 32:8 at a pressure of 5 torr. Multilayer graphene was synthesized with a H_2:CH_4 ratio of 1:9 at a pressure of 5 torr.

The VGScientia CVD furnace used a vertical gas flow direction, with gas entering from the top of the chamber and exiting at the base. In contrast to horizontal CVD furnaces whereby the copper substrate is oriented parallel to gas flow, in our system the copper is oriented perpendicular to the gas flow. This perpendicular nature means we have precise control of the effective amount of carbon and hydrogen radicals that the copper foil, as a whole, experiences simply by changing the z-height, pressure, and temperature within the furnace. Further, this enables homogenous growth over the whole copper foil, rather than heterogeneity across the length of the foil often observed in horizontal CVD furnaces. In the experiments, the increase in pressure (from 4 to 5 torr) results in a higher concentration of carbon radicals at the surface of the copper foil, leading to layer initiation and outgrowth. Increasing the carbon radicals dramatically by increasing the H_2:CH_4 ratio at equivalent pressure then enables continued layer growth and the formation of multilayered graphene.

FET device and measurement: Field effect transistors (FETs) with large-area graphene channel were fabricated. Monolayer and bilayer graphene were transferred to a p-type Si substrate coated with thermally grown SiO_2 of a thickness of 90 nm, by etching the copper substrate. In details, the graphene-grown Cu foil was spin-coated with

polymetilmethacrylate (PMMA) using a 6% PMMA solution in anisole followed by overnight curing at room temperature. The spin speed was 7700 rpm. The PMMA/graphene/Cu stack was then placed into a 0.01 mg/mL ammonium peroxidisulphate, $(NH_4)_2S_2O_8$ solution overnight to etch the Cu foil. The etchant was then replaced with a fresh $(NH_4)_2S_2O_8$ solution to remove any Cu residue, resulting in a PMMA/graphene stack. The stack was then scooped and rinsed in clean water for three times, each time lasts 15 min to remove the residual ions of the etchant. A SiO_2-coated Si substrate (purchased from Graphene Supermarket) was cleaned by sonication in acetone, isopropanol and deionized water continuously followed by drying in nitrogen gas. The substrate with SiO_2 facing upwards was used to scoop the floating PMMA/graphene stack from the water and form a PMMA/graphene/SiO_2/Si stack followed by drying at 180 ^oC for 1 h. The drying process removes any water residue between graphene and substrate. To remove PMMA on the top of graphene, a dichloromethane was used to dissolve PMMA layer overnight at room temperature. The obtained graphene/substrate was then dried using nitrogen gas at room temperature. Source and drain electrodes were patterned to contact the graphene channel and the back-gated voltage was applied by placing a silver wire on the Si substrate. The FET device is placed on a stable workstation within a sealed acrylic box. All the tests are at room temperature.

Electrochemical cycling and SEI preparation: The as-grown graphene on copper was cut into a defined area (1✕1 cm) and transferred into a lithium half cell, with metallic lithium as the counter electrode and 1 M $LiPF_6$ dissolved in a mixture of ethylene carbonate (EC) and dimethyl carbonate (DMC) (v/v, 1/1) as the electrolyte, with Celgard 2500 membrane as the separator. R2032 coin cells were assembled in an argon-filled glove box. The amount of electrolyte is 60 μL. Galvanostatic charge/discharge cycling and the in-situ high frequency resistance tests were carried out over a set voltage range of 0.01-3 V vs Li^+/Li using a 580 Bcycle battery test system. Electrochemical impedance spectroscopy (EIS) was studied using a Solartron Analytical 1286 Interface and 1260 Frequency Response Analyser, an ac amplitude of

5 mV in the frequency range 65 kHz to 10 mHz was employed. All electrochemical tests were carried out at room temperature. After 100 cycles, the cells were open in the glovebox. The copper-graphene electrode was rinsed with EC/DMC (1:1, v/v) solvent by three times following by drying in vacuum at room temperature. In the rinsing residue electrolyte was removed whilst SEI is unsoluble.

Material characterization: Scanning electron microscopy (SEM) images were recorded on an LEO Gemini 1525 FEG. X-ray photoelectron spectroscopy (XPS) was measured using a Thermo Scientific K-Alpha instrument (hυ=1486.6 eV) in ultrahigh vacuum. Measurement of the carrier mobility of the graphene samples was carried out on a Hall effect measurement system (Lake Shore, 8400 Series). Atomic force microscopy (AFM) was carried out on Bruker Innova Atomic Force Microscope. The analysis of the AFM images was through a software of Gwyddion. The compositional depth profile of the samples and surface composition were characterized by means of time-of-flight secondary ion mass spectrometry (TOF-SIMS, ION-TOF GmbH, Münster, Germany) on a spatial area of 100✕100 μm. The sputter gun uses specific ion beam to remove the surface materials, allowing depth profiles to be probed. An electron gun was used to compensate for charging effects. The sample transfer from glove box to the instrument is though a vacuum container. All the measurements were carried out at room temperature.

Simulation:

Intercalation energy and Löwdin population analysis was carried out using JDFTx on graphene, bilayer graphene and graphite lithiated structures both solvated in dimethyl carbonate (DMC) and in a vacuum state. Löwdin population analysis is used to determine the oxidation states of the atoms in the structure, while the intercalation energy determines the energy of lithium in the structure compared to lithium in bulk lithium solid. The calculations used optimised structures determined by manually finding the structure at the energy minima and by using an L-BFGS optimisation algorithm.

Each calculation used 20 hartree plane wave energy cutoff and 100 charge density cutoff as recommended for the GBRV PBE pseudopotentials that were used[1]. The k point grid used for all calculations was 12 x 12 x 4. A Fermi Dirac smearing scheme was used for filling the electronic states with a smearing width of 0.01 hartree. An electronic self-consistent field algorithm was employed for electronic minimisation. A GGA energy functional correction developed by Grimme was used to correct for Van Der Waals forces [2].

For the solvated structures, the liquid was modelled using a non-linear polarizable continuum model (PCM) where the liquid is modelled as a dielectric cavity with the same non-linear dielectric properties of the DMC [3]. A GLSSA13 PCM was used which includes empirical data for the cavity tension[3]. The DMC solvent was assumed to have bulk fluid density.

Results and Discussions

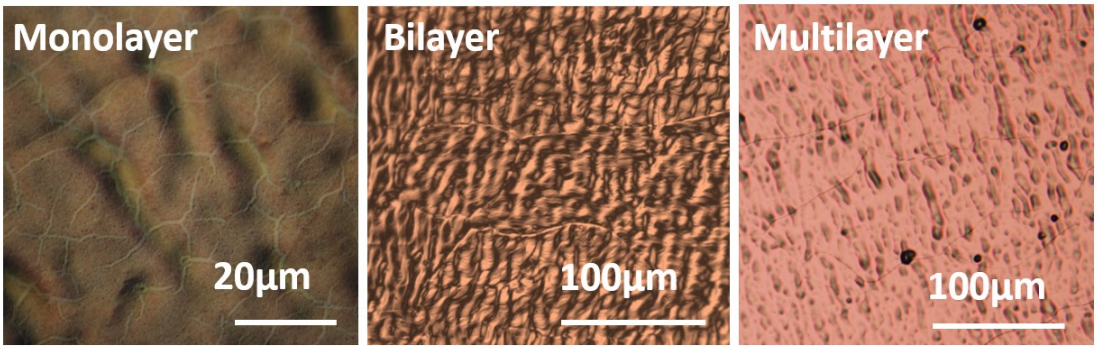

Figure S1 Optical microscopic images of graphene grown by CVD, from left to right: monolayer, bilayer and multilayer.

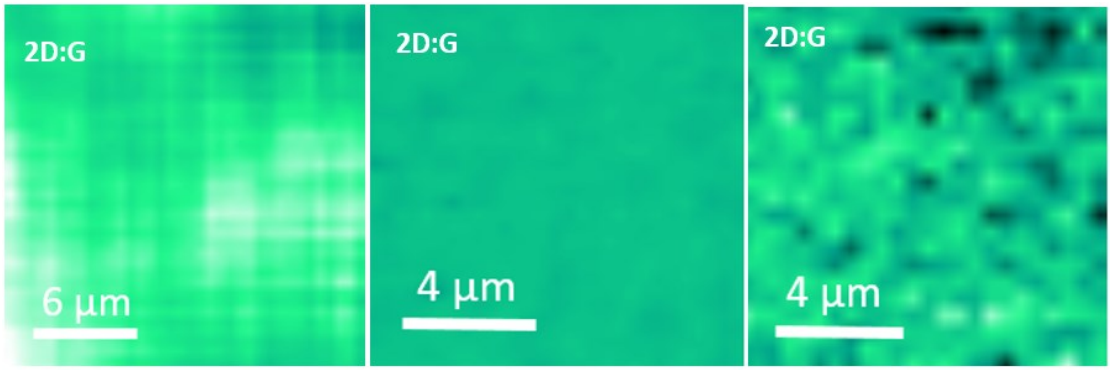

Figure S2 Raman mapping of the intensity ratio of 2D:G.

The optical micrographs of the three graphene samples on the copper substrate display the copper surface steps and graphene wrinkles which enlarge from mono- to multilayer (Figure S1). The graphene wrinkles are found to distribute across the whole copper surface and surface valleys, indicating a continuous film of graphene[4]. Raman spectroscopy which is sensitive to the geometric structure has been considered as the best technique to quantify the layer number of graphene[5] and the representative Raman spectra and mapping of these samples using a 514 nm laser excitation, are displayed in Figure 1a and b. The strong characteristic peaks are assigned to G (1580 cm^{-1}) and 2D (2670 cm^{-1}) bands, resulting from the in-plane vibration of sp^2 carbon atoms at the Brillouin zone center and the double resonance scattering of two phonons[6, 7], respectively. Both bands are highly sensitive to the layer number of graphene and display specific characteristics in the peak position and shape[6, 8-10]. The most significant factor, ratio of the intensity of 2D to G (I_{2D}/I_G) has been widely used to identify the layer number of graphene[7, 9, 11] and for our samples, monolayer graphene has I_{2D}/I_G ratio of ~2 and bilayer graphene ~1, which are typical features of mono-[4] and bilayer graphene[12]. A low I_{2D}/I_G ratio of 0.14, along with a shift in peak position from 2670 towards 2710 cm^{-1} signifies multilayer graphene or graphite[13, 14]. The corresponding Raman mapping of the I_{2D}/I_G ratio of each sample in Figure 1a indicates large areas of graphene with uniform layer number were grown via the large-scale CVD method directly on copper. Bilayer graphene shows the best uniformity in comparison with mono- and multilayer graphene which supports that when forming bilayer graphene by the CVD, two layers of graphene grow at the same time rather than via an underlayer mechanism[15].

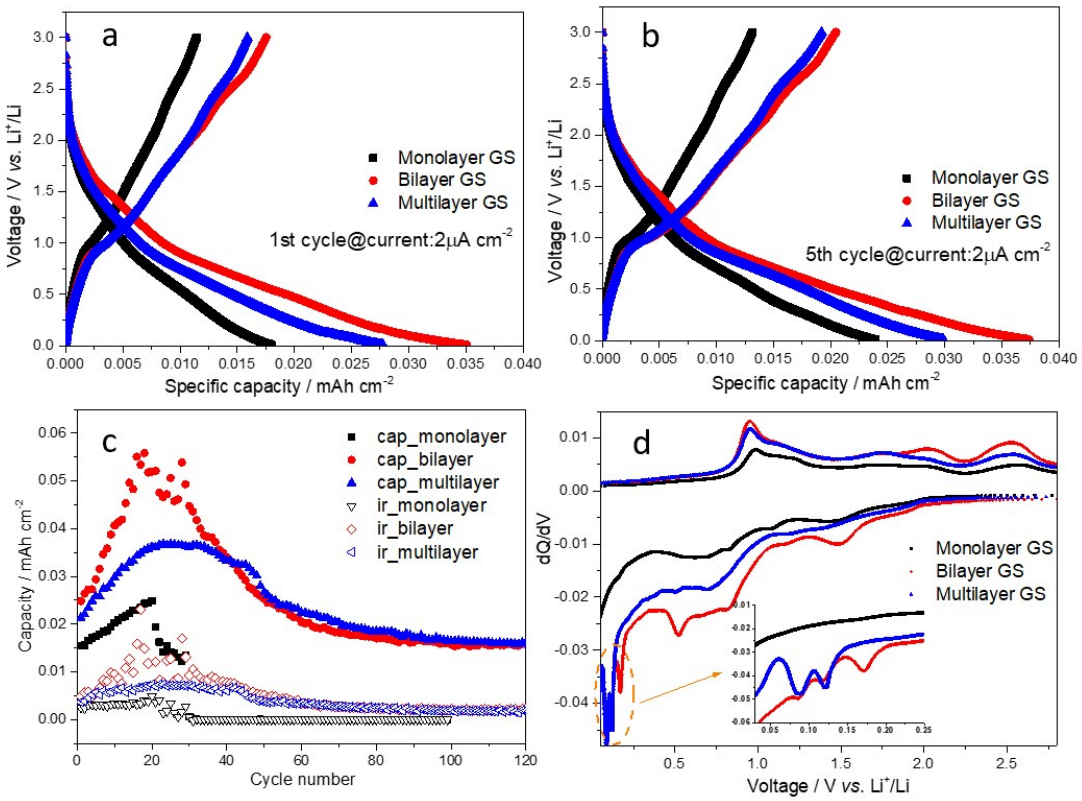

Figure S3 Electrochemical measurement of three graphene samples. Galvanostatic charge/discharge profiles at 2 μA cm^{-2} of (a) the first and (b) fifth cycle. (c) Irreversible capacity of mono-, bi- and multi-layer graphene in the lithium-ion cells with cycling in comparison with the discharge capacity. The discharged capacity is labelled with cap_ and irreversible capacity is labelled with ir_. Current density is 5 μA cm^{-2}. (d) dQ/dV vs. V curves of three samples of the first cycle. Current density is 2 μA cm^{-2}.

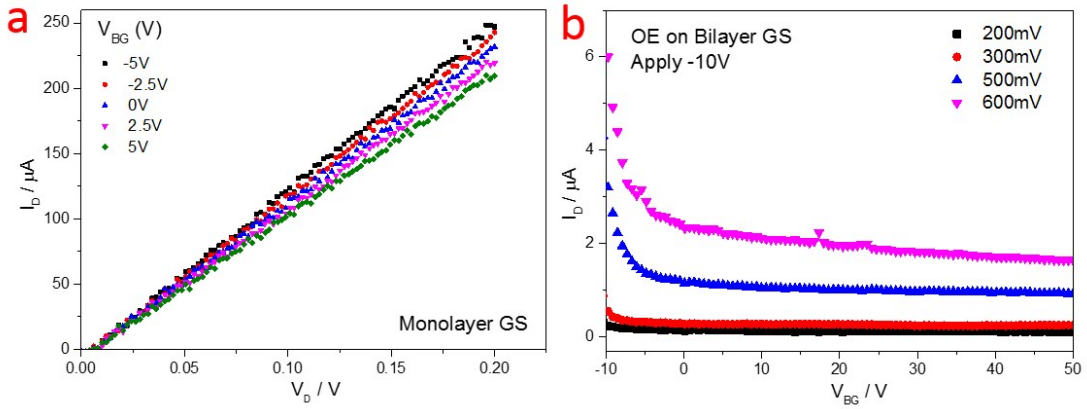

Figure S4 (a) Output characteristics of monolayer graphene. (b) Transfer characteristics of bilayer graphene with the organic electrolyte on surface and back gated at -10V for 5min. V_D is 200, 300 and 500 mV.

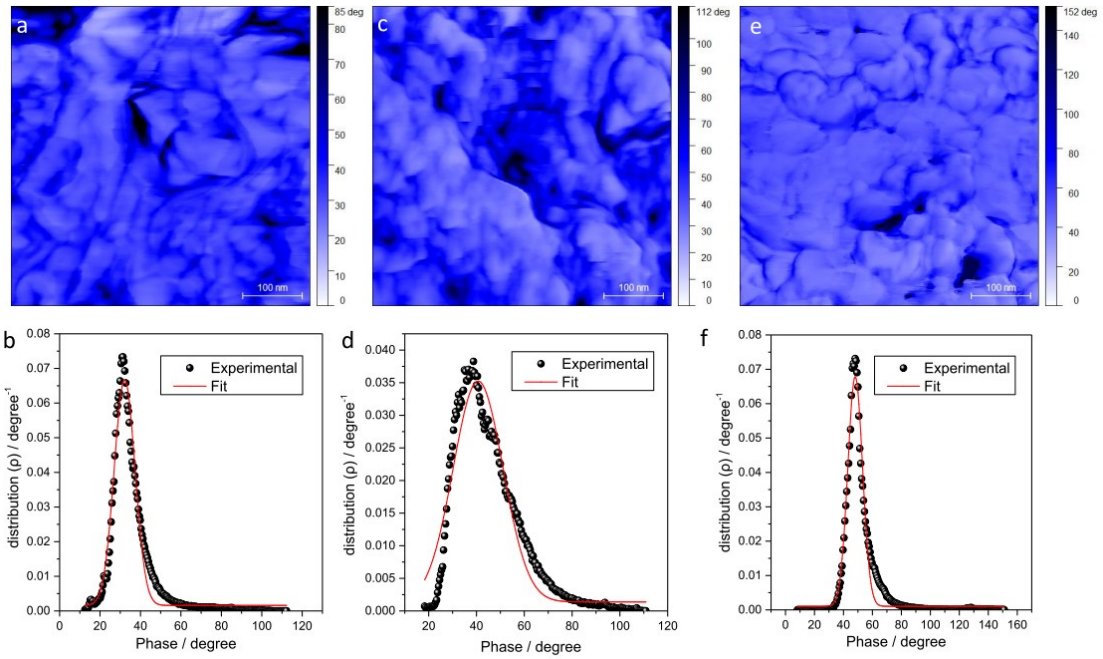

Figure S5 Phase-contrast AFM images and Gaussian distribution. (a, b) monolayer graphene, (c, d) bilayer graphene and (e, f) multilayer graphene.

Phase contrast AFM images indicate independent features to the topographical characteristics. The low contrast means small energy dissipation while high is large, corresponding to the low and high phase shift. The phase contrast indicates most of the analyzed surface is net repulsive ($\rho<90^{o}$) between the tip and sample. To compare the phase distribution of each sample, we use Gaussian function (equation S1) to fit the phase distribution spectra in each sample and obtain the center phase value and standard deviation.

$$f(x) = y_0 + a\exp[-(x - x_0)^2/b^2] \quad \text{(S1)}$$

The peak value is a risk for comparison because of the possible difference in the mechanical properties of the tip and thus the interaction with the sample surface. However, the phase contrast in one image is reasonable to compare and the standard deviation of each sample describes the distribution of the phase. The fitted results show the standard deviations of monolayer, bilayer and multilayer graphene are 7.27, 14.75 and 7.19 degree. Multilayer shows the most uniform phase contrast in these three samples.

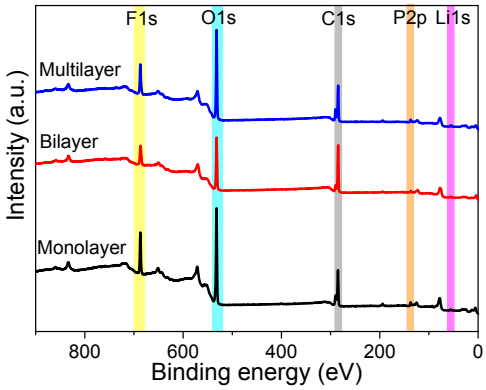

Figure S6 XPS survey spectra of the SEI films on the graphene samples.

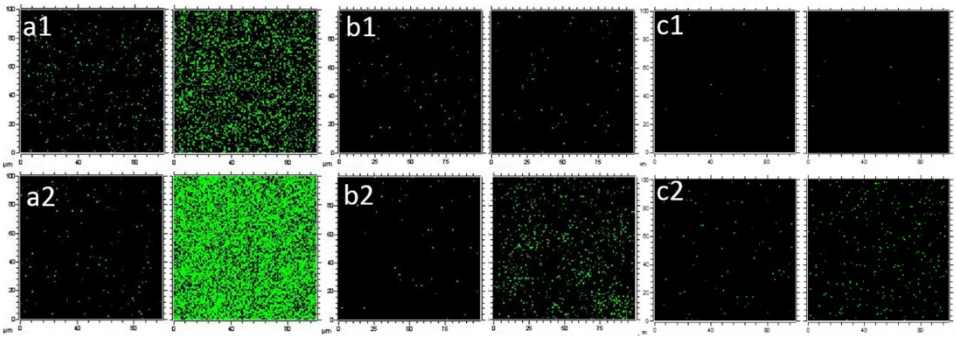

Figure S7 1 keV Cs^+ TOF-SIMS ion mappings of the SEI films on (a1-a2) monolayer, (b1-b2) bilayer and (c1-c2) multilayer graphene. The mapped ion fragments are (a1-c1) $PO_2F_2^-$ and (a2-c2) PO_3^- at the sputtering time of 0 (left side) and 40s (right side). The mapping color represents the dispersion of the secondary ions.

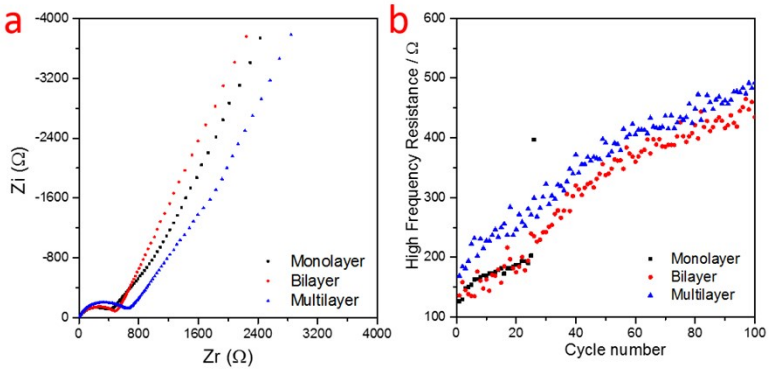

Figure S8 Electrochemical impedance of the graphene-Li half cell. (a) Nyquist plot of the cells after 10 cycles at a potential of 1.5 V vs. Li+/Li. (b) In-situ high frequency

resistance of the cells at 1000 Hz during cycling at 5 μA cm-2. Alternative current (AC) amplitude is 5 mV and interval time is 0.2 s.

Table S1 Parameters of pure phase used to calculate intercalation energies. Energy unit eV.

Structure	**C atoms**	**Li atoms**	**energy of all atoms**	**energy of all solvated**	**Energy in vacuum carbon/lithium**	**energy of solvated carbon/lithium**
monolayer	2	0	-11.427	-11.426	-5.7133	-5.7130
bilayer	4	0	-22.857	-22.856	-5.7143	-5.7141
multilayer	4	0	-22.861	-22.861	-5.7153	-5.7153
bulk Li	0	2	-14.395	-14.395	-7.1976	-7.1976

Table S2 Parameters of specific lithium-carbon layer structure used to calculate intercalation energies. Energy unit in eV. L and C mean lithium and carbon layer, LG is lithium-intercalated graphite (multilayer graphene).

Structure	***Number of Carbon atoms***	***Number of Lithium atoms***	***energy of vac (Hartree)***	***energy of sol (Hartree)***	***intercalation vac (eV)***	***intercalation sol (eV)***
LC	6	1	-41.467	-41.471	0.28369	0.11043
LCL	6	2	-48.656	-48.666	0.26132	0.09073
LCC	12	1	-75.756	-75.762	0.34192	0.13352
CLC	12	1	-75.797	-75.795	-0.77336	-0.77116
LCCL	12	2	-82.946	-82.961	0.27899	0.04333
LCLC	12	2	-82.985	-82.990	-0.25820	-0.34906
LCLCL	12	3	-90.173	-90.183	-0.08314	-0.19776
LG	6	1	-41.519	-41.519	-0.80824	-0.80764

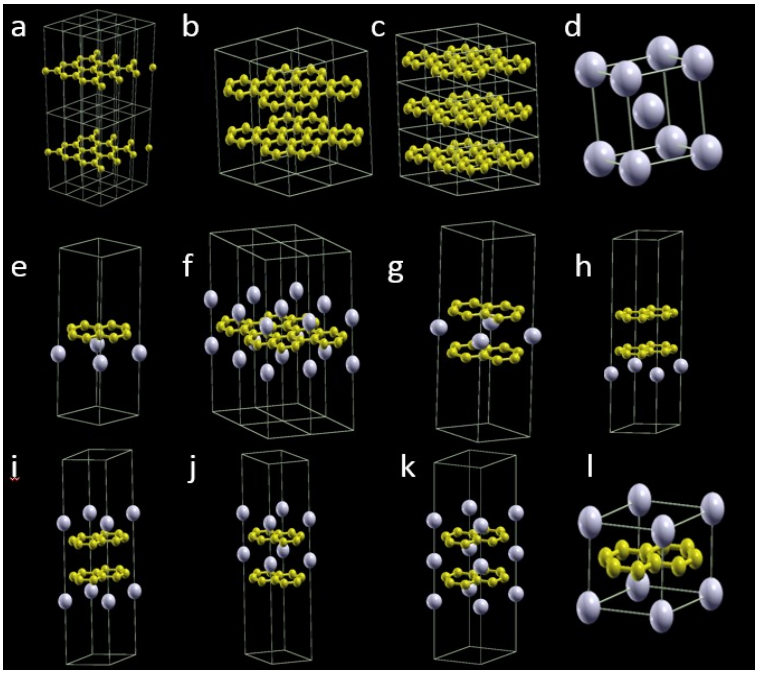

Figure S9 Model used in calculation. (a) monolayer, (b) bilayer with AA stacking, (c) graphite with AA stacking, (d) lithium bulk, (e-f) lithiated monolayer graphene, (g-k) lithiated bilayer graphene, (l) lithiated graphite.

Table S3 Calculated intercalation energy of the specific lithium-carbon layer structure in vacuum. Energy unit in eV. L and C mean lithium and carbon layer, LG is lithium-intercalated graphite (multilayer graphene).

Structure	Intercalation energy (eV)	Energy difference between consecutive structures	C/Li ratio
LG	*-0.80824*	*-0.03488*	*1*
CLC	-0.77336	-0.51516	2
LCLC	*-0.25820*	*-0.17506*	*1*
LCLCL	-0.08314	-0.34447	0.6667
LCL	*0.26132*	*-0.01766*	*0.5*
LCCL	0.27899	-0.00471	1
LC	*0.28369*	*-0.05822*	*1*
LCC	0.34192		2

Table S4 Calculated intercalation energy of the specific lithium-carbon layer structure in solvated system. Energy unit in eV. L and C mean lithium and carbon layer, LG is lithium-intercalated graphite (multilayer graphene).

Structure	*Intercalation energy (eV)*	*Energy difference between consecutive structures*	*C/Li ratio*
LG	-0.80764	-0.03647	1
CLC	-0.77116	-0.42210	2
LCLC	-0.34906	-0.15130	1
LCLCL	-0.19776	-0.24109	0.6667
LCCL	0.04333	-0.04740	1
LCL	0.09073	-0.01971	0.5
LC	0.11043	-0.02309	1
LCC	0.13352		2

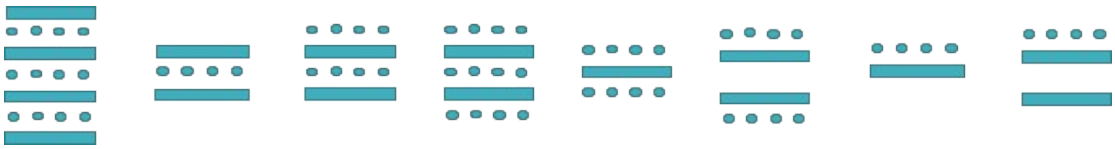

Figure S10 Order of the most energetically favourable structures depending on the intercalation energy in vacuum system. L denotes lithium ion layer and C is graphene layer. LG is lithiated graphite structure.

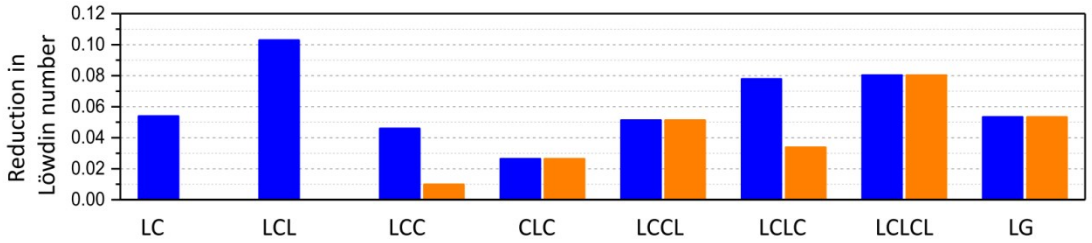

Figure S11 Quantified reduction of the oxidation state of carbon atoms (Löwdin number) in specific lithiated structure from the vacuum system.

References

1. Garrity, K.F., Bennett, J.W., Rabe, K.M. & Vanderbilt, D. Pseudopotentials for high-throughput DFT calculations. *Computational Materials Science* **81**, 446-452 (2014).
2. Stefan, G. Semiempirical GGA-type density functional constructed with a long-range dispersion correction. *J Comput Chem* **27**, 1787-1799 (2006).
3. Deniz, G., Kendra, L.-W., Ravishankar, S., Kathleen, A.S. & Arias, T.A. The importance of nonlinear fluid response in joint density-functional theory studies of battery systems. *Model Simul Mater Sc* **21**, 074005 (2013).

4. Li, X. et al. Large-Area Synthesis of High-Quality and Uniform Graphene Films on Copper Foils. *Science* **324**, 1312-1314 (2009).
5. No, Y.-S. et al. Layer number identification of CVD-grown multilayer graphene using Si peak analysis. *Sci Rep* **8**, 571 (2018).
6. Lin, S., Dong, L., Zhang, J. & Lu, H. Room-Temperature Intercalation and ~1000-Fold Chemical Expansion for Scalable Preparation of High-Quality Graphene. *Chem Mater* **28**, 2138-2146 (2016).
7. Calizo, I., Bejenari, I., Rahman, M., Liu, G. & Balandin, A.A. Ultraviolet Raman microscopy of single and multilayer graphene. *Journal of Applied Physics* **106**, 043509 (2009).
8. Ferrari, A.C. et al. Raman Spectrum of Graphene and Graphene Layers. *Phys Rev Lett* **97**, 187401 (2006).
9. Graf, D. et al. Spatially Resolved Raman Spectroscopy of Single- and Few-Layer Graphene. *Nano Lett* **7**, 238-242 (2007).
10. Ferrari, A.C. & Basko, D.M. Raman spectroscopy as a versatile tool for studying the properties of graphene. *Nat. Nanotech.* **8**, 235 (2013).
11. DasA et al. Monitoring dopants by Raman scattering in an electrochemically top-gated graphene transistor. *Nat Nano* **3**, 210-215 (2008).
12. Kim, D., Han, J.Y., Lee, D., Lee, Y. & Jeon, D.Y. Facile conversion of a cellulose acetate laminate film to graphene by a lamination process and post-annealing. *J Mater Chem* **22**, 20026-20031 (2012).
13. Shunyu, H. et al. Growth of low-threading-dislocation-density GaN on graphene by hydride vapor phase epitaxy. *Japanese Journal of Applied Physics* **56**, 030308 (2017).
14. Dai, G.-P., Wu, M.H., Taylor, D.K., Brennaman, M.K. & Vinodgopal, K. Hybrid 3D graphene and aligned carbon nanofiber array architectures. *RSC Adv* **2**, 8965-8968 (2012).
15. Shu, N. et al. Growth from below: bilayer graphene on copper by chemical vapor deposition. *New Journal of Physics* **14**, 093028 (2012).